 

PACS numbers: 42.55.Rz; 42.55.Xi; 42.60.Lh
DOI: 10.1070/QE2014v044n10ABEH015384

# Functional possibilities for forming different inverse population distributions in diode-side-pumped laser heads

S.G. Grechin, P.P. Nikolaev, E.A. Sharandin

*Abstract.* **The functional possibilities of diode-side-pumped laser heads of solid-state lasers for forming inverse population distributions of different types are analysed. The invariants determining the relationship between the laser head parameters upon scaling are found. The results of comparative experimental studies are presented.**

***Keywords:*** *laser head, diode side pumping, inverse population distribution, optimisation of parameters.*

## 1. Introduction

Pulsed flashlamps were used to pump the first solid-state lasers (SSLs) [1]. Their optimisation required new methods to design SSL laser heads. The development of diode pump sources provoked interest in laser heads [2] and stimulated researchers to optimse laser head parameters in order to implement these new possibilities, concerning both the efficiency and distribution of inverse population (IP) over the active-element (AE) cross section. Some studies aimed at optimising laser head parameters were carried out using purely experimental methods (see, e.g., [3–15]). Despite the fact that some properties of diode pump sources (low divergence and small spectral width) open radically new possibilities for obtaining IP distributions of different types, the purpose of most studies was to obtain a planar IP distribution over the AE cross section. This distribution is fairly universal and can be used to solve most of applied problems. Only few studies [3, 8] were aimed at forming an IP distribution similar to Gaussian (when focusing the pump beam on the AE axis), and certain attempts were made in [13] to obtain a distribution similar to parabolic.

Generally, an urgent problem is the simulation of pumping, which makes it possible to determine all functional possibilities of a laser head, as well as the optimal parameters of its elements for implementing a desired IP distribution. Some simulation results can be found, for example, in [16–39].

A model disregarding reflection and refraction at the AE surface was used in [16–21] for laser heads with a pump beam focused to the AE centre in order to form a Gaussian IP distribution; i.e., a problem of linear propagation of light through an absorbing medium was solved. In this consideration, the AE surface was assumed to be polished. Unidirectional pumping with a reflector placed on the AE external surface was used in [16–18]. The results of simulating laser heads with multiside pumped AEs are presented in [22–41]. Both diffuse (mostly) and mirror reflectors were considered. Among various problems in this field, two main directions can be selected as limiting cases: (i) formation of a flat (or similar to flat) IP distribution over the AE cross section [22–34] and (ii) formation of a convex (or similar to Gaussian) distribution [35–39].

A general feature of all studies in this field is the use of pump ray tracing. However, in practically all publications, the main features of propagation of partial rays from a pump source on their full path (until complete absorption) are not described. In addition, the reflection and refraction from all surfaces of the elements, scattering from matte surfaces, and specific features of propagation of different polarisation components are disregarded. A general description of the calculation technique and the calculation relationships for the IP formation, with allowance for all the aforementioned mechanisms, are presented in [33].

In most cases, calculated IP distributions over AE cross section are not compared with experimental data; only a purely qualitatively comparison can be found in some studies [28, 31, 34, 36, 38]. Obviously, the fact that the calculation results and experimental data are in only qualitative agreement is due to the large number of assumptions in the models used. We should note only study [27], where good agreement was obtained between the calculation and experiment.

An IP distribution desired for a particular practical application was obtained in most cases. A general analysis of the functional possibilities for forming IP distributions of different types over the AE cross section has not been performed; correspondingly, the parameters of laser head elements allowing for implementing these distributions have not been determined. Exceptions are studies [13, 28, 30–34, 39], where IP distributions for different parameters of elements are presented. However, the results obtained were discussed only qualitatively in these publications. Generally, the functional dependences setting a relationship between the parameters of laser head elements and the parameters for which optimisation was performed were not reported either. Thus, there is no complete information about the possibilities of diode-side-pumped laser heads in the literature.

In this paper, we analyse the functional possibilities of forming IP distributions of different types in cylindrical AEs. The problem of optimality of a particular IP distribution for lasing is beyond the scope of this study; it calls for a separate consideration.

**S.G. Grechin, P.P. Nikolaev, E.A. Sharandin** N.E. Bauman Moscow State Technical University, 2-ya Baumanskaya ul. 5, 105005 Moscow, Russia; e-mail: paneeque@gmail.com

Received 20 January 2014; revision received 20 May 2014
Kvantovaya Elektronika **44** (10) 912–920 (2014)
Translated by Yu.P. Sin'kov

## 2. Physical model of side pumping of an active element

Most axisymmetric schemes of diode side pumping can be reduced to a generalised version, which is shown in a simplified form in Fig. 1. Its main elements are an AE, an optically transparent tube, a reflector and a diode pump source. A transparent tube is used because the AEs of side-pumped SSLs in most of applications call for water cooling. In this case, the tube plays a role of an additional optical element. The reflector serves to return back to the AE the part of pump radiation that was not absorbed in the previous pass through the AE. The reflector contains entrance slits, through which the pump radiation arrives at the AE.

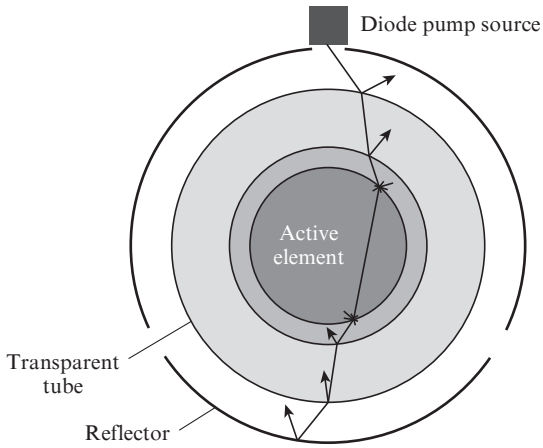


**Figure 1.** Generalised schematic diagram of diode side pumping.

The AE length in side-pumped laser heads is generally much larger than the AE transverse sizes. In addition, the pump absorption profile along the element optical axis is fairly uniform in most cases. Therefore, the consideration of AE pumping in one plane (perpendicular to the AE axis) is quite justified. In the design analysed here, the pump source can be considered as a point one in the two-dimensional approximation (at a small size of the emitting aperture). The pump radiation intensity, depending on the propagation angle, changes according to the normal law [42]:

$$I(\theta) = I(0)\exp\left[-\ln 2\left(\frac{\theta}{\theta_p}\right)^2\right], \quad (1)$$

where $\theta_p$ is the half-width of the pump divergence angle (at a level of 0.5).

The physical model based on the results of [33] uses a set of partial rays, propagating at different angles in the range from $-3\theta_p$ to $+3\theta_p$. Practically all pump radiation (more than 95%) is concentrated in this angular range. Each ray is routed through all optical elements and laser head units until its intensity reduces to a specified value (from $10^{-5}$ to $10^{-6}$ of the initial value). The propagation of a partial ray is considered taking into account the following physical mechanisms, properties and processes.

(1) Absorption of radiation in all optical elements and units according to the Bouguer law [42]:

$$I(x) = I(0)\exp(-\alpha x), \quad (2)$$

where $\alpha$ is the absorption coefficient and $x$ is the distance at which absorption occurs.

(2) Reflection and refraction of light at interfaces between media, depending on the light polarisation, in accordance with the Fresnel formulas [42]:

$$R_s = \left(\frac{\sin(\theta_i - \theta_t)}{\sin(\theta_i + \theta_t)}\right)^2 - \text{for s polarisation}, \quad (3)$$

$$R_p = \left(\frac{\tan(\theta_i - \theta_t)}{\tan(\theta_i + \theta_t)}\right)^2 - \text{for p polarisation}, \quad (4)$$

where $\theta_i$ is the angle of incidence of a ray at the interface between media and $\theta_t$ is the ray refraction angle.

(3) Total internal reflection at the interface between media, depending on the light polarisation.

(4) Scattering and depolarisation of light at diffuse and matte surfaces.

To calculate the IP distribution, the AE cross section is divided into elementary areas, and the absorption in each area is calculated independently. The fraction of absorbed radiation is determined according to the Bouguer law at a distance passed by a partial ray over a specific elementary area. Ray tracing is performed for several components of the pump emission spectrum. The accuracy of the calculation results depends on the number of spectral components. For all other optical elements the fraction of absorbed radiation is calculated integrally for the entire AE. The value of the absorption coefficient of the material corresponds to the centre pump wavelength. Scattering and depolarisation of light at diffuse and matte surfaces is simulated by the Monte Carlo method. The results of measuring the scattering diagrams of matte surfaces with different roughnesses are used in the model.

The laser head parameters are described using the following characteristics of the main laser head units. Pump source: centre radiation wavelength, $\lambda_p$; spectral width, $\Delta\lambda_p$; diameter of the circumference containing pump sources, $D_p$; pump beam divergence angle, $2\theta_p$; and light beam polarisation. Active element: absorption spectrum, $\alpha(\lambda)$; activator concentration, $C_{ae}$; diameter, $D_{ae}$; roughness of the lateral cylindrical surface, $Rz$; and refractive index, $n_{ae}$. Transparent tube: external and inner diameters, $D_{tub1}$ and $D_{tub2}$; roughnesses of the external and internal cylindrical surfaces, $Rz_1$ and $Rz_2$, respectively; refractive indices of the tube material and coolant, $n_{tub}$ and $n_{col}$; and absorption coefficients of the tube material and coolant, $\alpha_{tub}$ and $\alpha_{col}$. Reflector: reflection coefficient, $R_r$; diameter, $D_r$; input-window width, $s$; and surface roughness, $Rz_r$.

One of the purposes of simulating pumping is to calculate the pump absorption distribution in the AE at specified initial parameters. In this case, the output parameters of the complex simulation problem are the integral efficiency of pump energy absorption in the AE and the absorbed energy distribution in the AE volume.

The pump-energy absorption efficiency determines the total laser head efficiency and makes it possible to find the energy stored at the upper AE laser level (storing efficiency) and the small-signal gain.

The absorbed-energy distribution over the AE cross section determines two factors (which, in turn, characterise the energy and spatial parameters of lasing): IP distribution and, correspondingly, the gain distribution in the AE; the heat release distribution in the AE volume and, as a result, the refractive index inhomogeneities (thermooptical distortions) in the cw and repetitively pulsed regimes.

The main criterion for optimising a laser head is the maximum efficiency of pump energy absorption at specified IP and heat release distributions. Here, we consider only the functional possibilities of forming IP distributions of different types. The feasibillity of forming distributions of thermooptical distortions is a subject of separate publication.

Special software has been developed based on the above-described physical model; its interface is shown in Fig. 2. This software allows one to set all main parameters of elements and units of a diode-side-pumped laser head, perform two- and three-dimensional visualisation of calculation results and calculate functional dependences. All theoretical results presented below were obtained using this software.

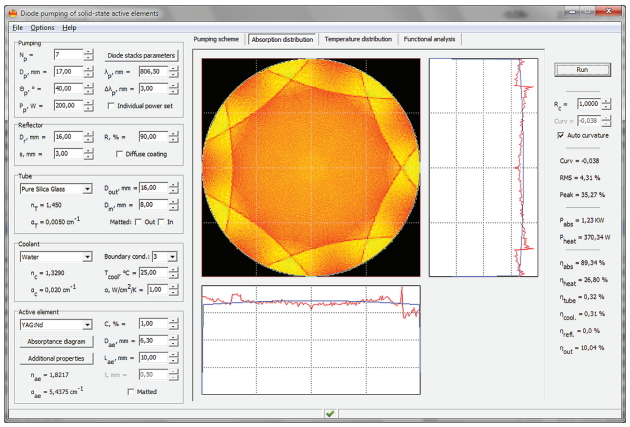

**Figure 2.** Software interface.

One of the main problems in designing a diode-pumped laser head is to optimise its parameters in order to obtain a desired IP distribution in the AE. Various SSL applications put different requirements to this distribution. To determine it (as well as the distribution of thermooptical distortions), one must generally solve the inverse problem of forming energy and spatial laser characteristics in the cavity. This is an independent problem, which specifies requirements to laser head parameters; however, it is beyond the scope of our study. As practice shows, among all possible versions, the most interesting are monotonic axisymmetric IP distributions, which are described by a parabolic function in a polar coordinate system (Fig. 3):

$$Q(r) = Q(0)(1 + pr^2), \tag{5}$$

where $p$ is the parabola curvature parameter and $r$ is the relative radius.

A more illustrative parameter, which describes parabolic distributions, is the centre-to-periphery drop of the IP density, which is related to the parabola curvature:

$$\delta = Q(0)/Q(1) = 1/(1 + p). \tag{6}$$

The correspondence between the calculated and model distributions is estimated using the standard deviation from the specified distribution according to the expression

$$\sigma = \sqrt{N}\frac{\sqrt{\sum(Q_i - Q_i^*)^2}}{\sum Q_i^*}, \tag{7}$$

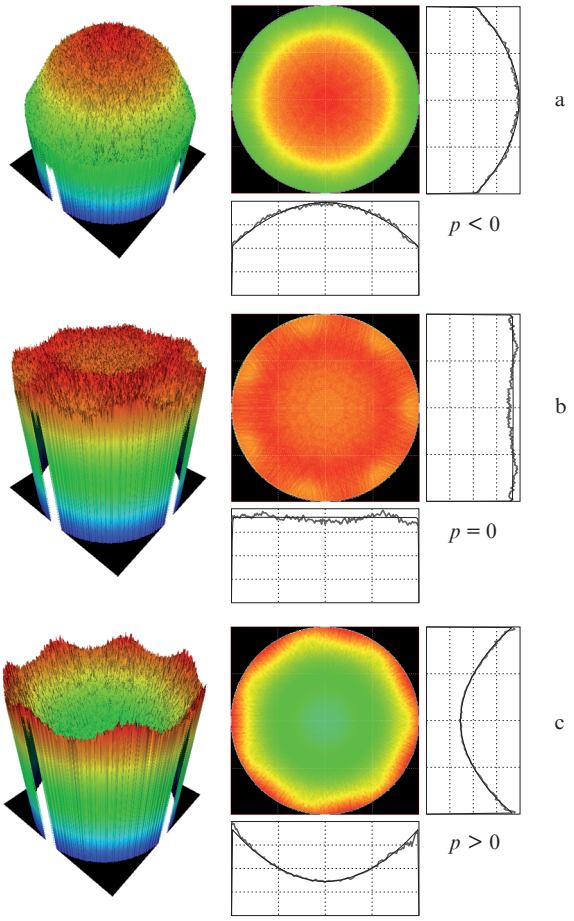


**Figure 3.** Parabolic IP distributions over the AE cross section with different curvatures $p$.

where $N$ is the number of counts in the distribution, $Q_i$ are the counts for the calculated distribution, and $Q_i^*$ are the counts for the specified distribution.

Distributions may contain large amplitude spikes, the so-called hot points, which cannot be taken into account using the standard deviation parameter if their number is small. In this case, one must use the parameter of maximum amplitude spikes for estimation:

$$\Delta_{\max} = N\frac{\max(Q_i - Q_i^*) - \min(Q_i - Q_i^*)}{\sum(Q_i - Q_i^*)}. \tag{8}$$

## 3. Analysis of functional relationships between laser head parameters. Invariants of parameters

Simulation of transverse AE pumping involves a large number of free parameters; in addition, many physical processes and mechanisms must be taken into account. Therefore, one of the main problems of theoretical analysis is the search for complex parameters (invariants), which describe laser heads with identical integral output parameters. Invariants establish a relationship between the parameters of laser head elements that allow one to perform generalised analysis of distributions formed and laser head scaling.

A simple geometric analysis of the paths of rays from the pump source through all optical elements of the laser head (disregarding the AE absorption) suggests the following basic

conclusion. The pump absorption efficiency in the AE and the IP distribution in it depend on the ray-path density, which determines the proximity of the paths of rays from the pump source to the AE axis; this characteristic can be described by the parameter

$$Inv_1 = \frac{D_p \sin\theta_p}{D_{ae}}. \quad (9)$$

This relation can also be presented as the ratio of the transverse size of the pump spot in the AE to the AE transverse size. The smaller this ratio, the higher the pump absorption efficiency is obtained in the AE (as well as the smaller the distance between the ray paths is and the more convex IP distribution is obtained in the element) and vice versa.

In practice, the AE absorption coefficient affects primarily the light absorption efficiency and the IP distribution. It is convenient to perform estimations using a universal parameter, which is independent of the pump source type and the AE type: the effective integral absorption coefficient $\varkappa$, which is defined as the overlap integral of the pump source spectrum and the AE absorption spectrum:

$$\varkappa = \frac{\int P(\lambda)\alpha(\lambda)\,d\lambda}{\int P(\lambda)\,d\lambda}, \quad (10)$$

where $P(\lambda)$ is the pump intensity and $\alpha(\lambda)$ is the AE absorption coefficient.

The characteristic distance at which pump radiation is absorbed is the AE diameter. Therefore, the laser head efficiency and the IP distribution in the AE can be determined by one more parameter, which was widely used when designing laser heads with flashlamp pump sources [43]:

$$Inv_2 = \varkappa D_{ae}. \quad (11)$$

An analysis of the results of numerical calculations of transverse AE pumping shows that $Inv_1$ and $Inv_2$ are invariants of laser head parameters. Provided that other parameters are the same, laser heads with identical $Inv_1$ and $Inv_2$ values (independent of the combinations in which the parameters enter them) have identical energy absorption efficiencies and identical IP distributions.

Let us now consider the results of the numerical analysis of the functional dependences by an example of YAG:$Nd^{3+}$ AE. For a single pump source, the IP distribution along the pump beam propagation direction is always descending. When there are several pump sources, these distributions are summed in the intersection regions. Figure 4 shows the IP distribution in AE at $Inv_1 = 1.0$ and $Inv_2 = 3.0$ and different numbers of pump sources $n$ (in the absence of a reflector). It can be seen that the IP distributions become more uniform with an increase in the number of pump sources and practically stop changing beginning with some $n$ value. This holds true for any pair of $Inv_1$ and $Inv_2$ values, which determine only the minimum number of sources necessary for uniform distribution. In most cases, for the optimal values of these parameters, the minimum necessary number of sources is 7. Specifically this number of sources will be used in the calculations below.

According to the calculation results, introduction of a reflector into the pump scheme does not affect much the character of the IP distribution but increases the pump absorption efficiency (Fig. 5), which depends primarily on the $Inv_2$ value. The reason is that the reflector and pump sources are generally located in the same circumference; therefore, the geometric path of rays through all optical elements of the laser head after reflection practically repeats their path prior to reflection. However, the presence of a reflector and its characteristics affect small-scale inhomogeneities of the IP profile (hot points).

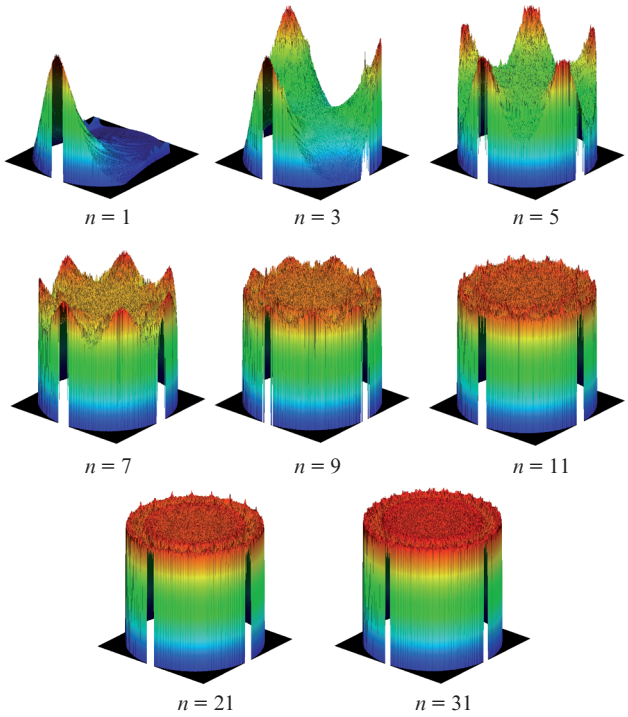


**Figure 4.** IP distributions over the AE cross section for different numbers of pump sources at $Inv_1 = 1.0$ and $Inv_2 = 3.0$.

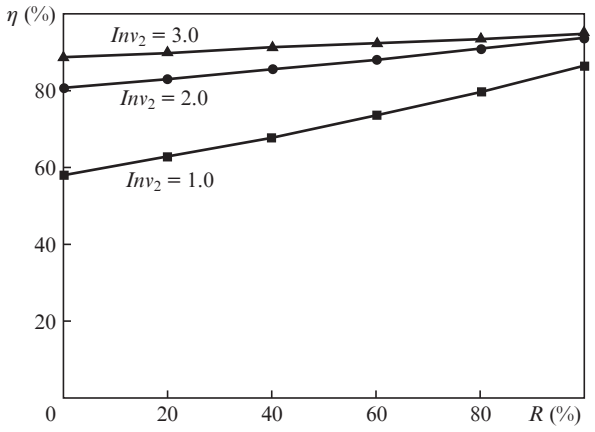


**Figure 5.** Dependences of the pump absorption efficiency on the reflection coefficient of the reflector at $Inv_1 = 1.0$ and different $Inv_2$ values.

The influence of the width of entrance slits in the reflector on the pump absorption efficiency is demonstrated in Fig. 6. The pump source is placed at a distance of 0.5–1.0 mm from the tube surface. Radiation vignetting reduces the efficiency for narrow slits. The pattern of the IP distribution changes as well. The effective area of reflector decreases with increasing

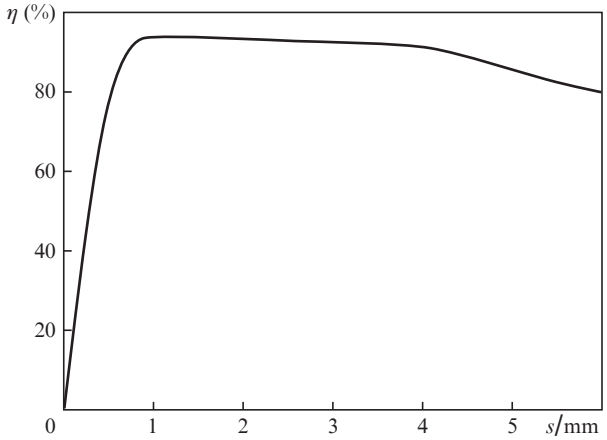


**Figure 6.** Dependence of the pump absorption efficiency on the width of the reflector input slits at $Inv_1 = 1.0$ and $Inv_2 = 3.0$.

slit size. The optimal slit size is chosen as a boundary value, after which the efficiency begins to fall more rapidly.

Matting of the AE and glass tube lateral surfaces or the use of a diffuse reflector decreases the energy absorption efficiency and makes the IP distribution more uniform. Figure 7 shows the calculated IP distributions for polished and matte (treated by M28 abrasive) AEs. Matting of this type reduces several times the distribution inhomogeneity.

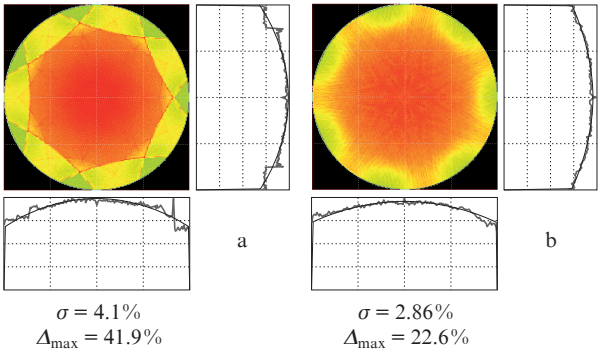


**Figure 7.** IP distributions over the AE cross section for (a) polished and (b) matte elements.

The first complex parameter $Inv_1$ is determined by the diameter of the circumference on which the pump sources are located, as well as the AE diameter and pump beam divergence. Table 1 contains IP distributions and energy absorption efficiencies for pumping by seven sources with a reflector, for different combinations of $D_p$, $D_{ae}$, and $2\theta_p$ that yield identical $Inv_1$ values. With a change in $D_{ae}$ the $\varkappa$ value changed correspondingly to retain the $Inv_2$ value invariable. These results show that the IP distribution and energy absorption efficiency are identical for the same $Inv_1$ values, provided that the other laser head parameters are identical. This result, observed independently of the set of other initial parameters, confirms that $Inv_1$ is an invariant of laser head parameters.

Below we present similar results for the second complex parameter $Inv_2$, which is determined by the AE diameter and effective absorption coefficient $\varkappa$ (it is directly proportional to the activator concentration $C_{ae}$). According to expression (10),

**Table 1.** IP distributions and energy absorption efficiencies for different combinations of $D_p$, $D_{ae}$ and $2\theta_p$.

| $Inv_1$ | $D_{ae}$/ mm | $D_p$/ mm | $2\theta_p$/ deg | $Inv_2 = 2.0$ Profile | $Inv_2 = 2.0$ $\eta$ (%) | $Inv_2 = 3.0$ Profile | $Inv_2 = 3.0$ $\eta$ (%) |
|---|---|---|---|---|---|---|---|
| 1.0 | 5.0 | 15.0 | 40 | 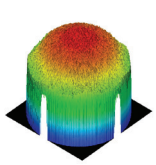 | 82.8 | 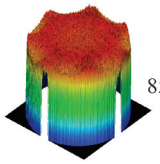 | 85.0 |
| | 7.0 | 27.0 | 30 | 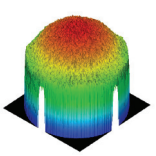 | 83.7 | 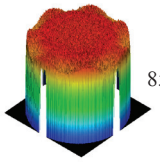 | 85.6 |
| 2.0 | 5.0 | 24.0 | 50 | 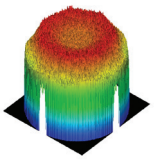 | 51.5 | 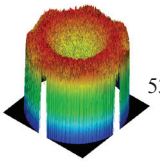 | 53.0 |
| | 7.0 | 28.0 | 60 | 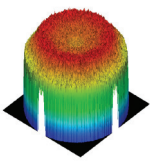 | 52.1 | 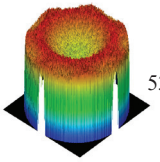 | 53.4 |

the effective absorption coefficient is determined by the AE absorption spectrum and the pump emission spectrum (specifically, by the centre wavelength and spectral width). Figure 8 shows the dependence of the effective absorption coefficient on the pump wavelength at different widths of the emission spectrum for an YAG:$Nd^{3+}$ AE with an activator concentration of 1.0%; the real absorption spectrum of the AE is considered. It is preferable to use radiation sources with a wider spectrum in laser heads. In this case, the laser head characteristics are more stable to temperature variations. The desired value of the effective absorption coefficient can be chosen by changing the activator concentration in the AE.

Table 2 contains IP distributions and energy absorption efficiencies in the case of a pump scheme with seven sources

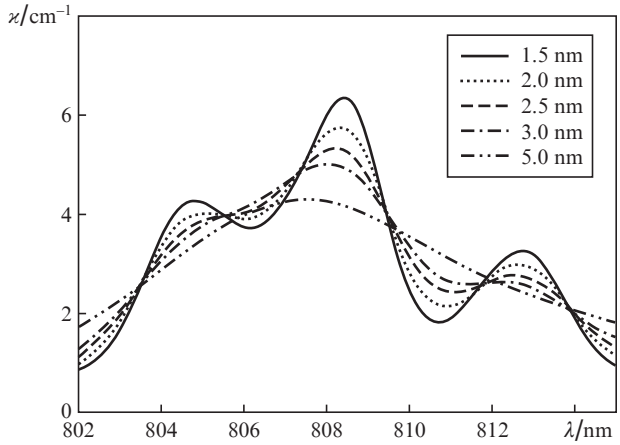


**Figure 8.** Dependences of the effective absorption coefficient on the pump wavelength at different pump spectral widths for an YAG:$Nd^{3+}$ AE with an activator concentration of 1.0%.

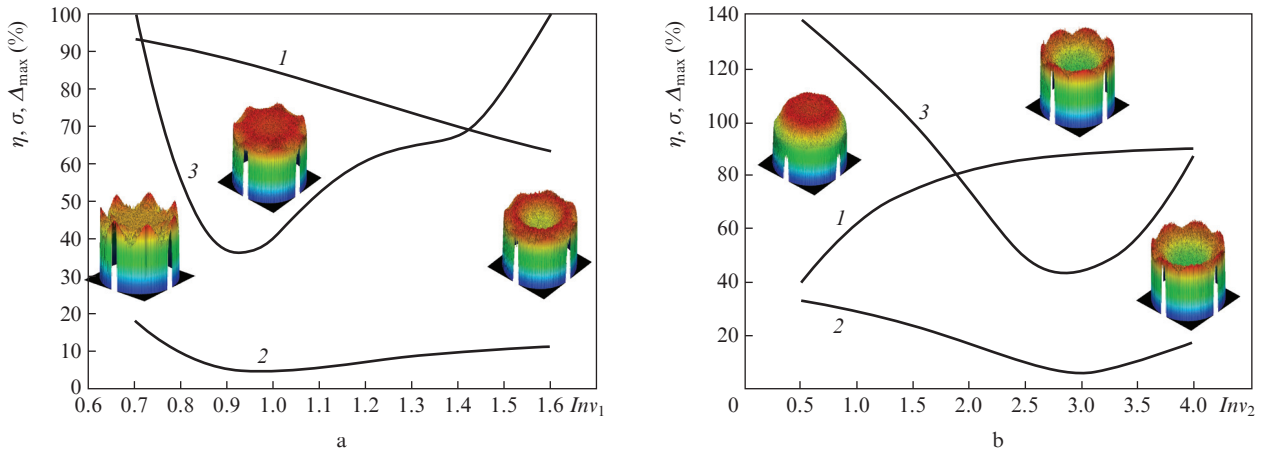


**Figure 9.** Dependences of the (*1*) light absorption efficiency, (*2*) standard deviation and (*3*) maximum spike amplitude on (a) $Inv_1$ at $Inv_2 = 3.0$ and (b) $Inv_2$ at $Inv_1 = 1.0$. For clarity, the IP distributions in the AE for specific $Inv_1$ and $Inv_2$ values are presented.

**Table 2.** IP distributions and energy absorption efficiencies for different combinations of $D_{ae}$ and $\varkappa$.

| $Inv_2$ | $D_{ae}$/ mm | $\varkappa$/ cm$^{-1}$ | $Inv_1 = 0.5$ Profile | $\eta$ (%) | $Inv_1 = 2.5$ Profile | $\eta$ (%) |
|---|---|---|---|---|---|---|
| 1.0 | 5.0 | 2.0 | | 82.8 | | 40.6 |
| | 7.0 | 1.4 | | 83.5 | | 40.6 |
| 4.0 | 5.0 | 8.0 | | 97.2 | | 44.5 |
| | 7.0 | 5.7 | | 97.6 | | 44.3 |

and a reflector, for different combinations of $D_{ae}$ and $\varkappa$, which yield the same value of the parameter $Inv_2$. When changing $D_{ae}$, the $D_p$ value was changed correspondingly to retain the $Inv_1$ value. The results show that the IP distribution and energy absorption efficiency are identical for the same $Inv_2$ values, with other laser head parameters chosen arbitrarily. This result is independent of the set of other initial parameters. Thus, we can conclude that $Inv_2$ is also an invariant of laser head parameters. As was mentioned above, to choose optimal values of invariants, one must use the criterion of the maximum pump absorption efficiency at a specified IP distribution. The degree of correspondence between the distribution obtained and the desired one is characterised by the standard deviation and maximum spike amplitude $\Delta_{max}$. Let us consider as an example the choice of optimal values of invariants for obtaining a uniform IP distribution.

Figure 9 shows functional dependences of the pump absorption efficiency, as well as the standard deviation and maximum spike amplitude, for the IP distribution in AE. The pump efficiency monotonically decreases with increasing $Inv_1$ and decreasing $Inv_2$, whereas the standard deviation and the maximum amplitude of separate spikes have practically coinciding minima. The optimal value of the invariants lies specifically in the vicinity of minimum in the standard deviation distribution. The results for an arbitrary set of laser head parameters are similar. The optimal values of $Inv_1$ and $Inv_2$ for a uniform IP distribution are, respectively, 1.0 and 3.0.

The search for optimal values of invariants is a two-parameter problem. For any set of laser head parameters and a specified IP distribution, the value of standard deviation and maximum spike amplitude have one global minimum in the functional dependence on $Inv_1$ and $Inv_2$. Figure 10 shows this two-parameter dependence of standard deviation for a flat distribution profile. This character of the dependence allows one to use one-dimensional functional dependences (as in Fig. 9) to search for optimal invariants.

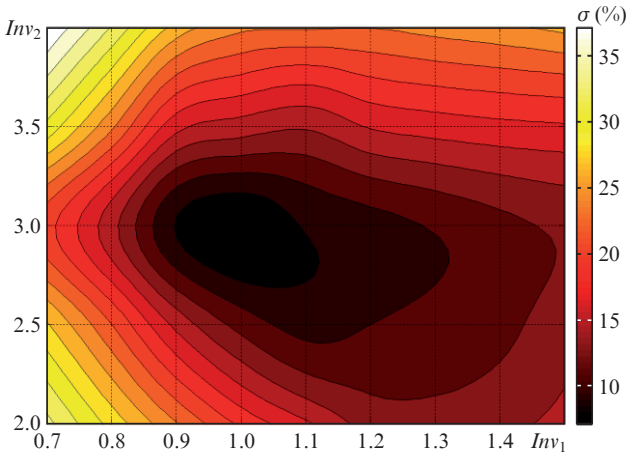


**Figure 10.** Two-parameter dependence of the standard deviation on $Inv_1$ and $Inv_2$ for a flat distribution profile.

There are specific pairs of optimal invariant values for different profiles of absorbed energy distributions. Figure 11 shows the optimal values of invariants $Inv_1$ and $Inv_2$ for different parabolic profiles of the energy absorbed in AE, characterised by a quantity $\delta$ (6).

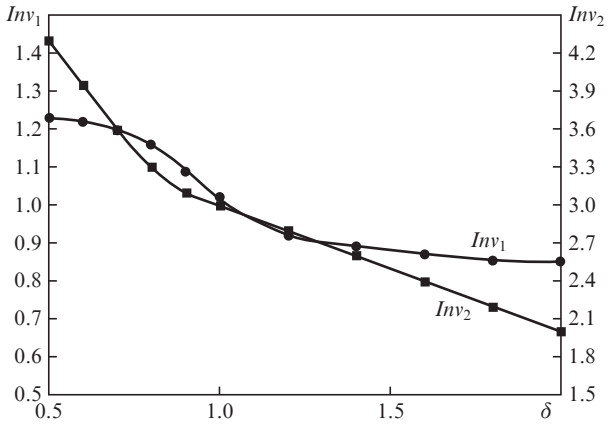


**Figure 11.** Dependences of the optimal values of invariants on parameter $\delta$ for parabolic distributions of the energy absorbed in AE.

## 4. Comparison of experimental data with calculation results

### 4.1. IP distribution over the AE cross section

One can only indirectly estimate experimentally the IP distribution (for example, from the luminescence intensity distribution over the AE cross section). Experiments were performed using an AE from an YAG:$Nd^{3+}$ crystal (with a diameter of 6.0 mm and an activator concentration of 1.1%) and tubes (with diameters of 19, 23 and 27 mm) having a reflecting coating on the external surface. Seven pump units were located on the AE perimeter. The pump beam divergence was 40°. Measurements were performed in the range of pump wavelengths from 803.9 to 808.6 nm; the pump spectral width was 1.7 nm. To reduce the influence of the luminescence amplification, the light scattered from the matte generatrix surface of the AE, and the diffraction effects, the luminescence intensity was measured at low pump currents, short AE illumination length and, correspondingly, a medium with a low gain.

Table 3 contains measured luminescence intensity distributions and calculated IP distributions in the AE for different $Inv_1$ and $Inv_2$ values. The experimental data are in good agreement with the calculation results; in addition, they justify the use of the proposed invariants to optimise laser head parameters. The experiments showed that one can change the transverse IP distribution at the AE centre in wide limits (from minimum to maximum) by changing the pump wavelength and reflector diameter.

Note that the luminescence intensity distribution does not completely correspond to the IP distribution in the AE: it is more smoothed and averaged, because it is the integral luminescence intensity distribution from the illuminated AE region that is experimentally recorded. In addition, the luminescence intensity is maximal at the periphery due to the scattering and diffraction of light from the AE lateral surface.

**Table 3.** Distributions of the measured luminescence intensity (E) and calculated IP (C) over the AE cross section for different $Inv_1$ and $Inv_2$ values and an AE with a diameter of 6.0 mm and activator concentration 1.1%. The curvature of the corresponding parabolic profile is indicated in each image [see (5)].

| $Inv_1$ ($D_{tub1}$) | $Inv_2 = 0.9$ ($\lambda$ = 803.9 nm) | $Inv_2 = 1.2$ ($\lambda$ = 805.2 nm) | $Inv_2 = 1.4$ ($\lambda$ = 807.2 nm) | $Inv_2 = 1.9$ ($\lambda$ = 808.6 nm) |
|---|---|---|---|---|
| 1.1 (19 mm) | E –0.323<br>C –0.318 | E –0.095<br>C –0.103 | E 0.062<br>C 0.061 | E 0.357<br>C 0.346 |
| 1.3 (23 mm) | E –0.227<br>C –0.220 | E 0.007<br>C –0.009 | E 0.110<br>C 0.108 | E 0.408<br>C 0.397 |
| 1.5 (27 mm) | E –0.155<br>C –0.150 | E 0.079<br>C 0.084 | E 0.140<br>C 0.133 | E 0.437<br>C 0.428 |

### 4.2. Pump absorption efficiency

The second laser head characteristic under consideration – pump absorption efficiency – cannot be measured directly. One can estimate it only indirectly in terms of the laser head gain characteristics, which make it possible to determine the absorbed and stored energies.

The laser head gain characteristics in the single-pass regime were measured using a master oscillator based on a passive $Q$-switched microchip YAG:$Nd^{3+}$ laser (1.064 μm). The master oscillator output radiation was single-mode and single-frequency; the pulse energy and width were 0.3 mJ and 0.7–1.0 ns, respectively; and the beam diameter was 0.8 mm. A telescope with a magnification of 2.5× was installed at the master oscillator output. Accordingly, the beam diameter at the amplifier input was 2 mm. The amplifier was designed based on a diode-side-pumped laser head; the AE was a YAG:$Nd^{3+}$ crystal 6.0 mm in diameter, with an activator concentration of 1.1%. The parameters of the laser head under study were the same as in Section 4.1. The pump energy of the amplifier was 280 mJ.

The small-signal gain was measured at two working temperatures: the optimal temperature (at which the gain reached maximum) and a temperature higher by 8 °C. The invariants of the laser head parameters at the optimal temperature were $Inv_1 = 1.0$ and $Inv_2 = 2.4$. The change in temperature by +8 °C

corresponds to a change in the pump wavelength by approximately 2 nm. Calculations show that this change leads to an increase in the effective pump absorption coefficient in the AE from 4.0 to 6.2 $cm^{-1}$ and in $Inv_2$ from 2.4 to 3.7. In accordance with the general properties (see above), the IP distribution becomes more uniform and the absorbed energy density at the AE centre decreases with increasing total absorbed energy of light throughout the entire AE volume. Since the amplified beam passes through the paraxial AE region, this effect reduces the gain.

The AE gain $k$ in the pumped region and the average stored energy density $Q_{st}$ in the AE region limited by the amplified-beam size are determined in terms of the small-signal gain $G_0$ as

$$k = \frac{1}{L_p}\ln G_0 + \beta\frac{L_{ae}}{L_p}, \tag{12}$$

$$Q_{st} = (\ln G_0 + \beta L_{ae})\, Q_{sat}, \tag{13}$$

where $L_{ae}$ = 120 mm is the AE length; $L_p$ = 10 mm is the length of pumped AE region, $\beta_{ae}$ = 0.008 $cm^{-1}$ is the absorption loss factor in the AE, and $Q_{sat}$ = 0.58 J $cm^{-2}$ is the saturation energy density for YAG : $Nd^{3+}$ [44] (this value was chosen based on experiments and results of lasing simulation).

Table 4 contains measured values of the small-signal gain $G_0$ and calculated values of gain $k$ of the medium and stored energy density $Q_{st}$ at the AE centre for the two aforementioned temperatures.

**Table 4.** Small-signal gains, gains of the medium, and stored energy densities.

| Temperature | $G_0$ | $k$/$cm^{-1}$ | $Q_{st}$/mJ $cm^{-2}$ |
|---|---|---|---|
| $T_{opt}$ | 1.47 | 0.48 | 280.2 |
| $T_{opt}$ + 8 °C | 1.39 | 0.42 | 247.5 |

The amplified-beam diameter was smaller than the AE diameter in our experiment; therefore, the gain characteristics were estimated from the average energy density stored in the central AE region, limited by the beam size. This estimate is sufficient for comparison with the calculation results, because previous measurements showed good agreement between the experimental and calculated IP distributions. If the pump energy and the distribution of the energy absorbed in the AE are known, one can estimate the average pump energy density for the central AE region, limited by the amplified-beam diameter:

$$\bar{Q}_p = E_p\eta_{abs}^{(c)}/S_b, \tag{14}$$

where $S_b$ is the area of the central AE region, limited by the amplified-beam diameter, and $\eta_{abs}^{(c)}$ is the fraction of the pump energy absorbed in the central AE region. The calculations were performed for $S_b$ = 0.03 $cm^2$ and $E_p$ = 280 mJ. At the optimal working temperature, $\eta_{abs}^{(c)}$ = 8.6%, whereas for a temperature changed by +8 °C, $\eta_{abs}^{(c)}$ = 7.3%.

Using expressions (13) and (14), one can estimate the energy stored in the central AE region:

$$\eta_{st} = Q_{st}/\bar{Q}_p. \tag{15}$$

The limiting efficiency of pump energy storage at the upper laser level, with allowance for the finite particle lifetime and the quantum defect of laser transition, is determined as

$$\eta_{st}^{(lim)} = \frac{1-\exp(-\tau_p/\tau_{up})}{\tau_p/\tau_{up}}\,\frac{\lambda_p}{\lambda_{gen}}, \tag{16}$$

where $\tau_{up}$ = 230 μs is the particle lifetime at the upper laser level, $\tau_p$ = 200 μs is the pump pulse width, $\lambda_p$ = 806.5 nm is the pump wavelength and $\lambda_{gen}$ = 1064.2 nm is the lasing wavelength. For these values, the limiting efficiency of pump energy storage throughout the total AE cross section was found to be 50.6%.

Using expressions (15) and (16), one can determine the pump absorption efficiency in the AE:

$$\eta_{abs} = \eta_{st}/\eta_{st}^{(lim)}. \tag{17}$$

Table 5 contains the values calculated using expressions (14), (15), and (17). The pump absorption efficiency is 71.8% for the optimal working temperature and 74.9% for the temperature increased by 8 °C. According to the calculation results, the absorption efficiency is 75.8% for the nominal working temperature and 78.2% for the temperature increased by 8 °C. The discrepancy in the experimental data and calculation results does not exceed 5%, which indicates that the theoretical model in use adequately describes the pump processes occurring in the laser head.

**Table 5.** Experimental and theoretical values of the pump absorption efficiency.

| Temperature | $Q_p$/mJ $cm^{-2}$ | $\eta_{st}$ (%) | $\eta_{abs}^{(exp)}$ (%) | $\eta_{abs}^{(th)}$ (%) |
|---|---|---|---|---|
| $T_{opt}$ | 771.6 | 36.3 | 71.8 | 75.8 |
| $T_{opt}$ + 8 °C | 652.7 | 37.9 | 74.9 | 78.2 |

## 5. Conclusions

The complete physical model of side diode pumping of cylindrical AEs, proposed in this study, is an efficient tool for designing laser heads. We considered the functional possibilities of forming IP distributions of different types in the AE and found the invariants determining the relationship between the parameters of laser head elements. The experimental data showed good agreement with the calculation results, in both the pump absorption efficiency and implemented IP distributions. We did not consider the problems related to the formation of thermo-optical phase inhomogeneities in the AE, which is a subject of a further study.

***Acknowledgements.*** We are grateful to A.V. Shestakov for his assistance.

This work was supported by the Russian Foundation for Basic Research (Grant Nos 12-02-01116 and 13-02-00667).

## References

1. Koechner W. *Solid-state Laser Engineering* (Berlin: Springer, 1999).
2. Grechin S.G., Nikolaev P.P. *Kvantovaya Elektron.*, **39**, 1 (2009) [*Quantum Electron.*, **39**, 1 (2009)].
3. Brioschi F., Nava E., Reali G.C. *IEEE J. Quantum Electron.*, **28**, 1070 (1992).
4. Shao J., Yang X., Geng A., Chen M. *Proc. SPIE Int. Soc. Opt. Eng.*, **7276**, 4 (2009).
5. Kojima T., Yasui K. *Appl. Opt.*, **36**, 4981 (1997).
6. Konno S., Yasui K. *Appl. Opt.*, **37**, 551 (1998).
7. Konno S., Kojima T., Fujikawa Sh., Yasui K. *Opt. Lett.*, **25**, 105 (2000).

8. Walker D.R., Flood C.J., van Driel H.M., Grenier U.J., Klingenberg H.H. *Opt. Lett*., **19**, 1055 (1994).
9. Greiner U.J., Klingenberg H.H., Walker D.R., Flood C.J., van Driel H.M. *Appl. Phys. B*, **58**, 393 (1994).
10. Yang X., Bo Y., Peng Q., Cui Q., Geng A., Cui D., Xu Z. *Chin. Opt. Lett*., **5**, 226 (2007).
11. Qian-Jin C., Qin-Jun P., Hong-Bo Zh., Xiao-Dong Y., Yong B., Xin-Jun G., Yong Zh., Yuan-Fu L., Da-Fu C., Zu-Yan X. *Chin. Phys. Lett*., **25**, 3991 (2008).
12. Moon H.-J., Yi J., Han J., Cha B., Lee J. *Appl. Opt*., **38**, 1772 (1999).
13. Sundar R., Ranganathan K., Nath A.K. *Opt. Laser Technol*., **39**, 1426 (2007).
14. Lee S., Yun M., Kim H.S., Cha B.H., Suk S. *Appl. Opt.*, **41**, 1082 (2002).
15. Yi J., Moon H.-J., Lee J. *Appl. Opt*., **43**, 3732 (2004).
16. Hanson F., Haddock D. *Appl. Opt*., **27**, 80 (1988).
17. Marshall L.R., Kaz A., Burnham R.L. *Opt. Lett*., **17**, 186 (1992).
18. Ajer H., Landr S., Rustad G., Stenersen K. *Opt. Lett*., **17**, 1785 (1992).
19. Sutton S.B., Albrecht G.F. *Appl. Opt*., **35**, 5937 (1996).
20. Xie W., Tam S.-Ch., Lam Y.-L., Liu J., Yang H., Gu J., Tan W. *Appl. Opt*., **39**, 5482 (2000).
21. Sovizi M., Massudi R. *Opt. Commun*., **275**, 206 (2007).
22. Jackson S.D., Piper J.A. *Appl. Opt*., **33**, 2273 (1994).
23. Brand T. *Opt. Lett*., **20**, 1776 (1995).
24. Jackson S.D., Piper J.A. *Appl. Opt*., **35**, 2562 (1996).
25. Du K., Zhang J., Quade M., Liao Y., Falter S., Baumann M., Loosen P., Poprawe R. *Appl. Opt*., **37**, 2361 (1998).
26. Takada A., Akiyama Y., Takase T., Yoshida Sh., Yuasa H. *Proc. SPIE Int. Soc. Opt. Eng.*, **3889**, 216 (1999).
27. Fujikawa S., Furuta K., Yasui K. *Opt. Lett*., **26**, 602 (2001).
28. Pavel N., Hirano Y., Yamamoto S., Koyata Y., Tajime T. *Appl. Opt*., **39**, 986 (2000).
29. Lee S., Choi D.W., Cha B.H. *J. Kor. Phys. Soc*., **49**, 430 (2006).
30. Liang D., Pereira R. *Opt. Commun*., **275**, 104 (2007).
31. Lee S., Kim S.K., Yun M., Kim H.S., Cha B.H., Moon H.-J. *Appl. Opt*., **41**, 1089 (2002).
32. Sabaghzadeh J., Rahimzadeh F., Mashayekhe I. *Opt. Laser Technol*., **40**, 748 (2008).
33. Wang Y., Kan H. *Opt. Commun.*, **226**, 303 (2003).
34. Wang Y., Kan H. *Opt. Lasers Eng*., **45**, 93 (2007).
35. Kasinski J.J., Hughes W., DiBiase D., Bournes P., Burnham R. *IEEE J. Quantum Electron*., **28**, 977 (1992).
36. Golla D., Knoke S., Schoene W., Ernst G., Bode M., Tunnermann A., Welling H. *Opt. Lett.*, **20**, 1148 (1995).
37. Golla D., Knoke S., Schone W., Bode M., Tunnermann A., Welling H. *Proc. SPIE Int. Soc. Opt. Eng.*, **2700**, 314 (1996).
38. Golla D., Knoke S., Schoene W., Ernst G., Tuennermann A., Welling H. *Proc. SPIE Int. Soc. Opt. Eng.*, **2379**, 120 (1995).
39. Meng J., Chen W., Hou X., Hu Q. *Chin. Opt. Lett*., **1**, 538 (2003).
40. Wang H., Huang W., Zhou Z., Cao H. *Chin. Opt. Lett.*, **1**, 541 (2003).
41. Sun Z., Li R., Bi Y., Yang X., Bo Y., Zhang Y., Wang G., Zhao W., Zhang H., Hou W., Cui D., Xu Z. *Opt. Commun*., **241**, 167 (2004).
42. Born M., Wolf E. *Principles of Optics: Electromagnetic Theory of Propagation, Interference, and Diffraction of Light* (Oxford: Pergamon, 1964; Moscow: Nauka, 1973)
43. Mikaelyan A.L., Ter-Mikaelyan M.L., Turkov Yu.G. *Opticheskie generatory na tverdom tele* (Optical Solid-State Oscillators) (Moscow: Sov. Radio, 1967).
44. Kaminskii A.A. *Laser Crystals* (New York: Springer, 1981; Moscow: Nauka, 1975).